LUND UNIVERSITY

Quantitative analysis of Cherenkov emission imaging

Master's thesis project, Spring 2012

Susanna Olausson

Supervisors:
Johan Axelsson
Sven-Erik Strand

Faculty of Science, Lund University
Department of Medical Radiation Physics
Clinical Sciences, Lund

Populärvetenskaplig sammanfattning

Avbildning genom detektion av Cherenkovstrålning är en nuklearmedicinsk bildtagningsmetod där man utnyttjar det synliga ljus som kallas Cherenkovstrålning. Detta ljus sänds ut när hastigheten hos en laddad partikel överstiger hastigheten av ljuset i ett visst medium och kan användas för att lokalisera fördelningen av en radionuklid i en kropp.

Syftet med denna studie är att undersöka möjligheten att kvantitativt analysera avbildning med Cherenkovstrålning för att avgöra huruvida metoden kan användas som ett dosimetriskt verktyg vid systemisk strålterapi.

Systemisk strålterapi är en metod för behandling av cancer där radioaktiva isotoper administreras till patienterna för att uppnå celldöd hos tumörcellerna. För att uppnå ett bättre resultat kan radioisotoperna märkas med en monoklonal antikropp som binder till receptorer hos cancercellerna. Vissa typer av cancerceller har visat sig överuttrycka vissa receptorer vilket gör det möjligt att rikta behandlingen mer direkt mot tumören.

För att säkerställa terapeutisk effekt måste man försäkra sig om att radioisotopen ackumuleras i tumören under en tillräckligt lång tid. Det är också viktigt att behandlingen är selektiv så att friska organ kan besparas onödig stråldos. Effektiviteten och specificiteten hos ett isotop-antikropp komplex undersöks rutinmässigt med prekliniska dosimetristudier.

Molekylär bildtagning med nuklearmedicinska bildtagningsmetoder som PET och SPECT möjliggör visualisering av cellfunktion och molekylära processer i levande organismer utan att störa dessa processer. De många modaliteterna inom fältet är applicerbara på bland annat diagnosticeringen av cancer, neurologiska sjukdomar och hjärt-kärlsjukdomar.

Optiska bildtagningsmetoder, såsom fluorescens- och bioluminescensbildtagning, är till skillnad från nuklearmedicinska bildtagningsmetoder lätta att hantera och instrumenten är mycket billigare än de som krävs för PET och SPECT. Av dessa anledningar föredrar många att använda sig av optiska bildtagningsmetoder för att undersöka molekylära processer vid grundläggande och biomedicinska studier. Optiska bildtagningsmetoder har hög känslighet och utmärkt tidsupplösning, men kvantifiering baserad på den optiska signalen är osäker. Metoderna har dock begränsad klinisk tillämpning på grund av absorption och spridning av ljuset när det passerar genom kroppen, vilket leder till låg penetration av vävnad.

På senare tid har det funnits ett ökande intresse för optiska tekniker för avbildning av radioisotoper, tekniker baserade på emission av Cherenkovstrålning. Det är av stort intresse att ytterligare undersöka möjligheten att använda sig av bildtagning med Cherenkovljus som ytterligare ett verktyg för preklinisk dosimetri.

Jämfört med kliniskt använda molekylära bildtagningsmetoder som PET och SPECT är Cherenkov-bildtagning en enkel och kostnadseffektiv bildtagningsmetod, vilket gör metoden intressant för exempelvis screening.

Avbildning med Cherenkovstrålning kan användas för att lokalisera radionuklider i prekliniska djurstudier, detta betyder att metoden skulle kunna användas för att studera selektivt upptag i ytliga tumörer.

Slutligen skulle denna bildtagningsmetod kunna utgöra ett alternativ till preklinisk PET, med lägre kostnad och högre genomströmning.

Abstract

Cherenkov emission imaging is a new optical imaging technique in nuclear medicine that takes advantage of the fact that most positron emitting radionuclides have a sufficient energy to produce Cherenkov photons. The Cherenkov photons can then be detected with sensitive CCD camera systems.

Due to the recent demonstration of detectable amounts of Cherenkov light escaping from nuclide bearing mice the interest in Cherenkov radiation has increased. The demonstrated results of animal studies give an implication that it is possible to use the CR phenomenon for medical research and possibly for clinical purposes.

A large plethora of clinically used radiopharmaceuticals for imaging and therapy can be imaged with Cherenkov luminescence imaging (CLI). This means that it is possible to use the method to follow the distribution of these radiopharmaceuticals in vivo, thereby the method could possibly be used as a dosimetry tool in systemic radiation therapy (SRT).

Several research groups have investigated the correlation between CLI and PET-imaging, and an excellent correlation between the bio-distributions obtained with the two methods has been found. Compared to currently used imaging methods such as PET and SPECT, CLI is a simple method which makes it interesting for e.g. screening purposes. The equipment needed for CLI is less expensive than PET and SPECT equipment, meaning that it would be a good alternate method for smaller laboratories with a restricted budget.

The aim of this study is to investigate the possibility for quantitative measurements and to quantitatively analyse the use of Cherenkov emission imaging in optical phantoms and pre-clinical animal models.

This study includes several experiments where the relation between different optical properties of the studied media and the emitted Cherenkov radiation is investigated. The results shown by the work in this thesis are in good agreement with the theoretical expectations and results shown by other research groups.

Cherenkov emission imaging can be used for radionuclide localization in preclinical animal studies, meaning that the method could be used to study selective uptake in superficial tumours. The CLI method could provide us with a low-cost high-throughput alternative to preclinical PET.

Contents

List of abbreviations

CCD – Charge Coupled Device

CLI – Cherenkov Luminescence Imaging

CR – Cherenkov radiation

FDG – Fludeoxyglucose

HER2 - Human Epidermal Growth Factor Receptor 2

keV – kilo electron volt

mAb – Monoclonal antibody

MBq – Mega Becquerel

PET – Positron Emission Tomography

RADAR – the RAdiation Dose Assessment Resource

SPECT – Single Photon Emission Computed Tomography

SRT – Systemic radiation therapy

UV – Ultra violet

1. Introduction

1.1 Motivation of the thesis

The aim of the work presented in this thesis is to quantitatively analyse the use of Cherenkov emission imaging in phantoms and pre-clinical animal models. The motivation of the work is to investigate the feasibility of Cherenkov emission imaging as a tool for dosimetry studies on systemic radiation therapy.

Cherenkov emission imaging is of great interest since it is a simple method compared to positron emission tomography (PET) and single photon emission computed tomography (SPECT). It is possible to use Cherenkov emission imaging as a simple screening instrument instead of more complicated methods.

Another interesting aspect is that the method allows for imaging of pure beta emitters, which is not possible with the pre-clinical methods used today.

1.2 Systemic radiation therapy

Systemic radiation therapy (SRT) is a cancer treatment modality in which radioactive isotopes are administered to patients in order to achieve tumour cell kill. To reach a better tumour cell kill the radioisotope can be labelled with a monoclonal antibody (mAb) that binds to specific receptors on the cancer cells. Some types of cancer cells have been shown to overexpress certain receptors, providing means for specific tumour targeting [1-3].

To be able to achieve therapeutic efficacy, one need to assure that a sufficient activity of the radioisotope is accumulated in the tumour for a sufficient period of time. It is also of great importance that the selectivity is high enough to spare healthy organs. The efficiency and the specificity of an isotope-mAb compound are routinely investigated in pre-clinical dosimetry studies [1-3].

A lot of the work that is done to develop new radiopharmaceuticals is based on preclinical animal studies. In this type of studies the distribution of the radiolabeled pharmaceuticals in the animals is investigated over time.

1.3 Molecular imaging in nuclear medicine

Molecular imaging with nuclear imaging modalities such as PET and SPECT enables visualization of cellular function and molecular processes in living organisms without perturbing them. The multiple and numerous potentialities of this field are applicable to the diagnosis of diseases such as cancer, neurological and cardiovascular diseases.

Optical imaging, such as fluorescence and bioluminescence imaging, is in contrast to nuclear imaging easy to handle and the instrumentation is less expensive than that of PET and SPECT. This is one reason why many basic and biomedical studies prefer optical imaging to examine molecular processes in living systems. Optical imaging methods have high sensitivity and excellent temporal resolution. However, quantification based on the optical signal is inaccurate and has limited applications in clinics due to the absorption and scattering of light in body and resulting low tissue penetration [4].

Recently there has been an escalating interest in optical techniques for radioisotope imaging [5] and electron beam imaging[6], techniques that rely on Cherenkov emission. Optical imaging, when compared to scintillation camera imaging, allows a higher throughput as more pre-clinical models can be imaged at the same time [7]. To investigate the potential of Cherenkov emission imaging as an additional tool for pre-clinical radioisotope dosimetry is of great interest.

Despite the influence of absorption and scattering, recent studies have shown satisfactory correlations between Cherenkov emission and PET signals using ^{18}F and ^{89}Zr. The limitations in sensitivity, caused by the diminished penetration depth due to scattering and absorption, limits the clinical use of Cherenkov emission imaging for whole body tomography. However, for preclinical studies Cherenkov emission imaging could provide a high-throughput precursor or validation method for in vivo PET studies [5].

2. Cherenkov emission

Cherenkov emission imaging is a simple imaging method compared to other molecular imaging methods that are currently used, such as PET and SPECT. This makes Cherenkov emission imaging an interesting method for e.g. screening purposes.

2.1 Historical background

Optical emission induced by relativistic particles was first described by Pavel Cherenkov in the early 1930s [6]. Cherenkov radiation (CR) is emission of visible light that occurs when a charged particle travels through a dielectric medium at a speed that exceeds the phase velocity of light in that medium. When these conditions are fulfilled a photonic shockwave is produced, this is comparable to the sonic shockwave associated with supersonic bodies in air [8].

In media such as biologic tissue and water the speed of light, v_n, is less than *c*. The reduction of the speed of light in a medium is due to the interaction of light with the material and is proportional to the refractive index of the medium according to Eq. (1) [5, 9].

$$v_n = \frac{c}{n} \tag{1}$$

When the speed of a particle nears the speed of light, the relativistic kinetic energy, E, is calculated according to Eq. (2) [5, 9].

$$E = mc^2 \left(\frac{1}{\sqrt{1 - \frac{v^2}{c^2}}} - 1 \right) \tag{2}$$

The required conditions for Cherenkov emission renders a threshold condition given by Eq. (3).

$$\beta \cdot n > 1 \tag{3}$$

In Eq. (3), n is the refractive index of the medium, β is related to the energy of the particle and defined by:

$$\beta = \left[1 - \left(\frac{1}{\frac{E_{(keV)}}{511} + 1} \right)^2 \right]^{\frac{1}{2}} \tag{4}$$

Eq. (4) is valid for an electron or a positron with the energy *E*, since 511 keV is the rest energy of one of these particles.

In water the threshold energy of electrons is 264 keV, while in tissue, assuming a refractive index of 1.4, the threshold energy is 219 keV. Several of the radioisotopes used in biomedical imaging satisfy the Cherenkov emission criterion given by Eq. (3) [6].

The Cherenkov photons are produced in a continuous spectrum from the near ultraviolet through the visible spectrum, with intensity inversely proportional to the square of the photon wavelength [5, 8, 10]. The data presented by Robertson et al. [5], see Figure 2.1, confirms that the produced light follows an inverse relationship with the square of the wavelength.

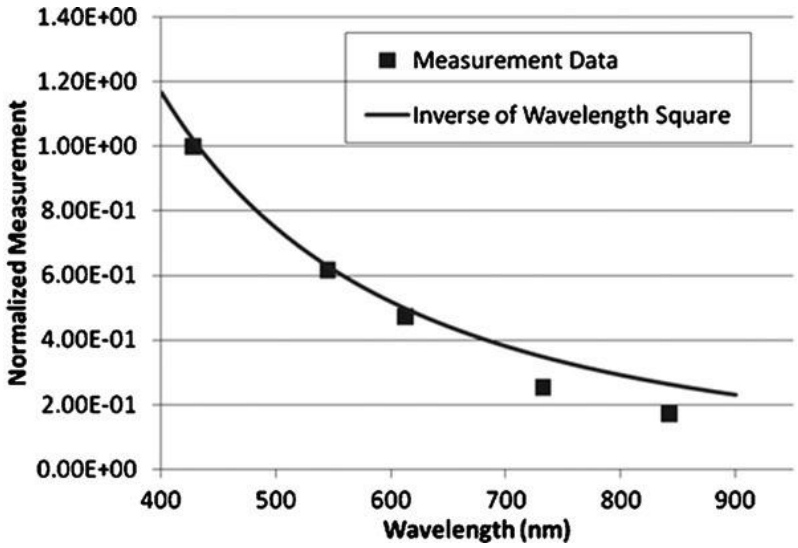

Figure 2. 1: Results from measurements made by Robertson et al. [5] showing that the intensity of the emitted Cherenkov radiation is inversely proportional to the wavelength.

The number of produced photons depends on the initial energy of the charged particle. Ross et al. [10] has calculated the Cherenkov photon yield in seven spectral regions for electrons with different energies ranging from 275 to 4000 keV, a selection of the calculated photon yields are tabulated in Table 2.1. The tabulated photon yields show that the higher initial energy a particle has the more photons it will generate before dropping below the Cherenkov emission threshold.

Table 2. 1: Cherenkov photon yields of electrons in water for selected spectral ranges adopted from Ross et al. [10].

	Photons/spectral region [nm]						
Electron energy [keV]	**250-300**	**300-350**	**350-400**	**400-450**	**450-500**	**500-550**	**500-600**
275	0,0032	0,0023	0,0017	0,0013	0,0011	0,0009	0,0007
300	0,0041	0,0029	0,0022	0,0017	0,0013	0,0011	0,0009
400	0,723	0,513	0,385	0,300	0,240	0,196	0,163
500	2,22	1,58	1,18	0,992	0,737	0,604	0,501
600	4,45	3,16	2,37	1,85	1,48	1,21	1,00
800	10,7	7,59	5,69	4,43	3,54	2,90	2,41
1000	18,9	13,4	10,0	7,82	6,25	5,12	4,25
2000	78,8	56,0	42,0	32,7	26,1	21,4	17,8
3000	160	114	85,1	66,3	53,0	43,4	36,0
4000	215	181	136	106	84,5	69,3	57,5

Several of the medical radioisotopes currently in clinical use emit beta particles with kinetic energies that fall within the range of Cherenkov photon generation, seen in Table 2.1. [9]. Thus, there is a potential application of Cherenkov emission in medical radionuclide imaging.

2.2 Cherenkov emission imaging of small animals

The recent increased interest in Cherenkov radiation is due to the demonstration of detectable amounts of light escaping from a radionuclide bearing live mouse, which implies that there is a possibility to utilize the CR phenomenon for medical research and perhaps for clinical purposes [8]. Cherenkov radiation from common PET nuclides has been detected in vivo in live mice using sensitive Charge Coupled Device (CCD) optical imaging systems [11].

Recently several groups, including Robertson et al. [5], Spinelli et al. [12] and Mitchell et al. [13] established an imaging approach called Cherenkov emission imaging (CLI) for in vivo imaging of small animals such as mice. Cherenkov emission imaging is based on detection of Cherenkov radiation generated by beta particles as they travel through tissue with an energy that satisfies the threshold condition for Cherenkov emission. In both the studies mentioned the possibility of detecting Cherenkov radiation escaping from mice injected with ^{18}F-FDG was investigated using widely available optical imaging instruments.

The bio-distribution of a large variety of radiopharmaceuticals for both therapy and imaging can be imaged using Cherenkov radiation eliminating the need for expensive dedicated SPECT or PET tomographs [12]. All currently used positron emitting radionuclides have a sufficient energy to produce Cherenkov radiation detectable with sensitive optical imaging equipment [5]. It has also been experimentally confirmed that Cherenkov radiation from beta emitters can be used as a quantitative and qualitative tool for assessment of radiotracer distribution in vivo [14].

The correlation between PET and Cherenkov emission imaging has been investigated by several groups that have performed longitudinal imaging studies. An excellent correlation between the bio-distributions obtained with CLI and commercial preclinical PET has been found. It has also been found that changes with respect to time, tumour model and radiopharmaceutical formulation are consistent in CLI and PET data [14-16].

The most commonly cited biomedical application of CLI is as a high throughput, low cost alternative to PET imaging, a method referred to as Cherenkov luminescence imaging [8]. The clinical use of CLI for whole body tomography will be restricted by the sensitivity limitations caused by scattering and absorption. For preclinical studies on the other hand, CLI could provide a high-throughput precursor or validation for PET studies in vivo [5].

A number of other possible applications for CR are suggested, applications such as using it as an alternative to bremsstrahlung for imaging of pure beta emitters or as an intra-operative or endoscopic imaging of targeted structures in humans. Other suggested applications are as an excitation source for different fluorophores, a higher resolution autoradiography method and as a light source for photodynamic therapy [8].

To sum it up it should, in principle, be possible to apply the CLI method to any radioisotope emitting charged particles with an energy that exceed the threshold energy for production of Cherenkov radiation in the media [11].

The big advantage with the CLI method is the possibility for cost-effective screening with high throughput. CLI could largely improve the throughput of current preclinical imaging since this method allows for imaging of 5 animals at the time with an integration time of 5 minutes, while PET allows for imaging of 1 or 2 animals per 10 minutes [7, 16].

Another advantage could be that the Cherenkov radiation is produced during the initial decay process, which makes it more localized to the actual decay event than the annihilation event tracked by PET imaging [5].

The CLI method is believed to progress rapidly because of the improvement in throughput in combination with sensitivity to therapeutic effect, decreased equipment cost and the many available nuclear probes. The lowered cost for imaging systems will allow the technique to spread to smaller laboratories with limited budget [12, 16, 17].

3. Light propagation in tissue

Light, which is propagating in biological tissue, will interact with the constituents of the tissue. The two primary ways of interaction are elastic scattering and absorption.

3.1 Absorption

Light can be absorbed if encountering an absorbing chromophore with a difference in energy between electronic states that matches the energy carried by the optical radiation. This spectrally dependent absorption forms the basis for a wide selection of applications. The transmitted intensity, I_T, decreases exponentially with the propagation distance, d, according to the Beer-Lambert law if the scattering of the light is negligible. The Beer-Lambert law is shown in Eq. (5).

$$I_T(\lambda) = I_0(\lambda) \cdot e^{-\mu_a d} \tag{5}$$

The absorption coefficient, μ_a, in Eq. (5) is stating the probability of absorption per unit length. The absorption coefficient is essentially the summation of all chromophore contributions and it is given by:

$$\mu_a(\lambda) = \sum_i \varepsilon_i(\lambda)[C_i] \tag{6}$$

In Eq. (6) ε_i is the extinction coefficient for chromophore *i* and C_i is the concentration of this chromophore. The scattering in biological tissue is normally higher than the absorption, resulting in that the Beer-Lambert law only can be applied with modifications and on certain occasions [18]. The main absorbing chromophores in biological tissues are listed below.

Haemoglobin

There are two forms of haemoglobin; oxygenated and deoxygenated. The spectral absorption characteristics for the two forms of haemoglobin are different and this can be used to assess the oxygenation of the tissue [19, 20]. The oxygenation of the tissue is a valuable tool in assessment of hypoxia since the status of a tumour can show oxygen deficiency.

Water

Water is present in abundance in the entire body and it is normally represented by the water fraction. The water mainly absorbs the light in the near infrared wavelength region.

Lipids

This is the family name for a variety of several different substrate types. One area where lipids play an important role is as building blocks in cell membranes. Like water, lipids absorb at longer wavelengths. Lipids are relatively weak absorbers compared to water [21].

Melanin

Is present in superficial skin where it acts as a protecting layer against the sun's ultra violet (UV) radiation; it is the melanin that is responsible for the colour of our skin. Melanin is not only found in the skin, it can also be found in for example the brain [22].

Myoglobin

There are two kinds of myoglobin; oxy- and deoxy-myoglobin, and the absorption characteristics are similar to the ones of haemoglobin. Myoglobin is primarily found in muscular tissues [23].

Cytochromes

Cytochromes are different substrates that reflect the mitochondrial content. Spectroscopic assessment of these substrates could render information about the metabolism of the studied medium[24].

3.2 Scattering

Cells with intracellular organelles and extracellular structures build up tissues. The structures of the cells form a complex matrix which macroscopically regulates the anatomy of the organs. The variety of cells throughout the body results in several different tissue types with different constituent composition. However, the origin of scattering is thought to be the same in the different tissue types. The scattering is due to the variation in refractive index within the medium [25].

Another property that affects the scattering is the size of the tissue components; the size distribution of tissue components range from nm-sized proteins to µm-sized cells. This fact has made it possible to use scattering-based diagnostic methods to probe morphological changes in the tissue [26, 27].

When the scattering properties are analysed theoretically one usually assume that the tissue components are spherically shaped particles. The Mie theory is then used to model the electromagnetic wave propagation. The scattering from one sphere can be described by the radiation caused by a dipole induced through the interaction with the incident electromagnetic field [28]. Scattering patterns from a limited number of spherical particles can very well be described by Mie theory, but the complexity of biological tissues makes it impractical to adopt in real applications.

In optical studies of tissue the macroscopic properties normally are of interest. Two physical quantities are defined; the scattering coefficient, μ_s, and the anisotropy factor, g.

$$g = \langle cos(\theta) \rangle \tag{7}$$

In Eq. (7) θ is the scattering angle and μ_s states the probability for scattering per unit length and g gives information about in what direction the light is scattered on average. Because of its composition, tissue has an anisotropy factor that is approaching unity, meaning that tissue is forward scattering. In highly scattering tissues the two quantities are combined into the reduced scattering coefficient, μ_s', which is shown in Eq. (8) [29].

$$\mu_s' = (1 - g)\mu_s \tag{8}$$

4. Cherenkov emission in optical phantoms

Experiments with optical phantoms were made to investigate how the radiance of the Cherenkov emission is affected by different properties of the imaged object.

4.1 Experimental setup

The experimental setup consists of a charge coupled device (CCD) camera (Andor iKon-M DU934P-FI) mounted with the objective lens (Schneider Kreuznach Xenon 25mm/0.95) inside a light tight enclosure. The CCD camera is also connected to a cooling system and a computer with the necessary imaging software to save and handle the images. A schematic view of the setup is shown in Figure 4.1.

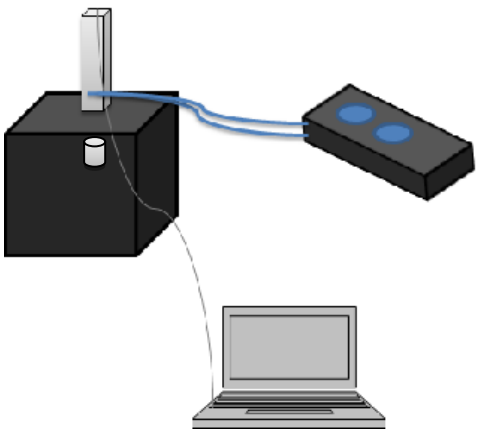

Figure 4. 1: A schematic image of the setup; to the left is the light tight enclosure in which the imaged objects were placed, to the right is the cooling system used to cool the camera and in the bottom of the figure is a laptop with imaging software.

During imaging the optical phantoms were placed in the light tight enclosure, the images were then acquired by the CCD which was cooled to between -65°C and -95°C. The phantoms were placed in the light tight enclosure to minimize the background light. To further suppress the background light the enclosure was covered with black fabric and the lights in the room were switched of during imaging.

In order to better understand the setup a schematic image of the inside of the light tight enclosure is presented in Figure 4.2 and a photograph of a well plate inside the enclosure is shown in Figure 4.3. Well plates are placed on a plastic block to be at the right distance from the lens, in the experiments where a test tube is used as an optical phantom the tube is attached to a sample holder on the millimetre screw in the corner of the enclosure. The millimetre screw allows for the sample to be raised or lowered from the outside without the need to open the enclosure.

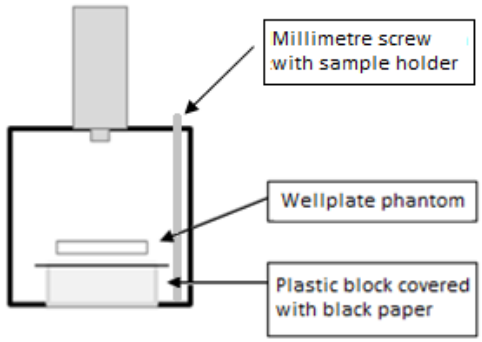

Figure 4. 2: A schematic image of the inside of the light tight enclosure with a well plate phantom placed on a plastic block. The plastic block is covered with black paper to ensure that all light in the images originates from the phantom and not from the plastic it is placed on.

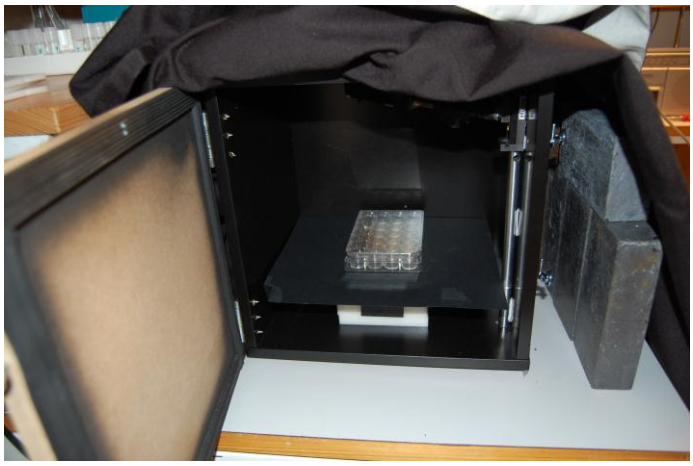

Figure 4. 3: A photograph of the light tight enclosure containing a well plate phantom. To the right one can see the millimeter screw used to change the distance between the test tube phantoms and the lens.

One type of optical phantom consists of well plates with different mixtures of, water, bovine blood and Intralipid-20%® in order to mimic the optical properties of different tissues. Intralipid-20%® is an emulsion of soy bean oil (20%), egg phospholipids, glycerine and water, that in our experiments is used as a scattering medium [30]. In figure 4.4 a photograph of the well plate with the different mixtures is seen, in addition all the different mixtures are displayed in Table 4.1.

Figure 4. 4: A photo of the type of well plate used, with the different mixtures of water, blood and Intralipid in the different wells.

Table 4. 1: The different content of water, blood and Intralipid in the wells of the well plate.

Mixtures		
Water volume [µl]	**Blood volume [µl]**	**Intralipid-20% volume [µl]**
1200	0	0
1200	5	0
1200	10	0
1200	20	0
1200	30	0
1200	0	40
1200	5	40
1200	10	40
1200	20	40
1200	30	40
1200	0	100
1200	5	100
1200	10	100
1200	20	100
1200	30	100
1200	0	175
1200	5	175
1200	10	175
1200	20	175
1200	30	175

The well plates with different mixtures of blood and Intralipid was used in the experiments where the effects of different optical properties were studied. In the experiments where the wavelength dependence was investigated the same mixture was used in all the wells.

The other type of optical phantom consists of a test tube containing a liquid solution with the radionuclide, and a larger container with different mixtures of water, bovine blood and Intralipid in which the test tube is lowered. A schematic of this setup is seen in Figure 4. 5.

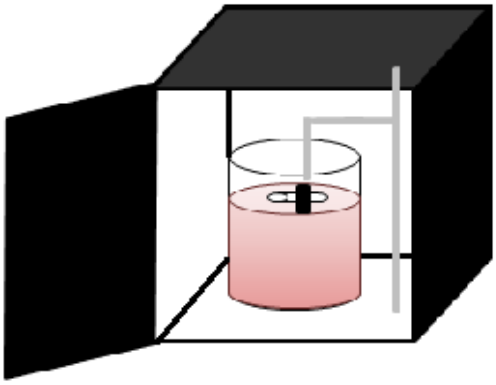

Figure 4. 5: A schematic image of the light tight enclosure containing the test tube mounted in the holder on the millimetre screw and lowered in a container with water, blood and Intralipid.

The setup shown in Figure 4.5 was used for the experiments investigating how the radiance is affected by the choice of radionuclide and the energy of the chosen nuclide. The effect of the depth of the test tube in the larger phantom is also studied.

4.2 Optical radiance as a function of activity

To investigate how the radiance is affected by the activity we prepared a well plate phantom and let it decay while placed in the light tight enclosure. The radionuclide used was ^{18}F, which has a half-life of approximately two hours, images were gathered every hour and the phantom was studied for about three half-lives.

The results of these measurements are shown in Figure 4.6; the figure shows the relationship between radiance and activity for the well containing only water. However our measurements showed a linear relation with different inclination for all the different mixtures of water, Intralipid and bovine blood. Our results are in agreement with the results shown by several other research groups, including Robertson et al. [5], Beattie et al.[8] and Xu et al.[9].

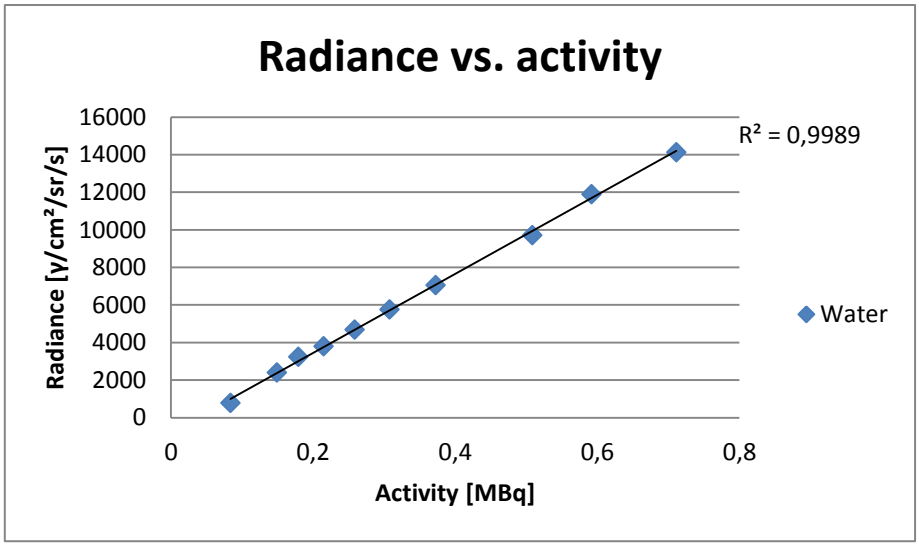

Figure 4. 6: Radiance as a function of activity for the ROI of the well plate containing only water.

In Figures 4.7 - 4.10 the mean radiance is plotted as a function of activity for all the different mixtures in the different wells and the relationship between radiance and activity was studied. The measurements show that all mixtures have a linear relationship between these properties, with different inclination for different concentrations of blood and Intralipid.

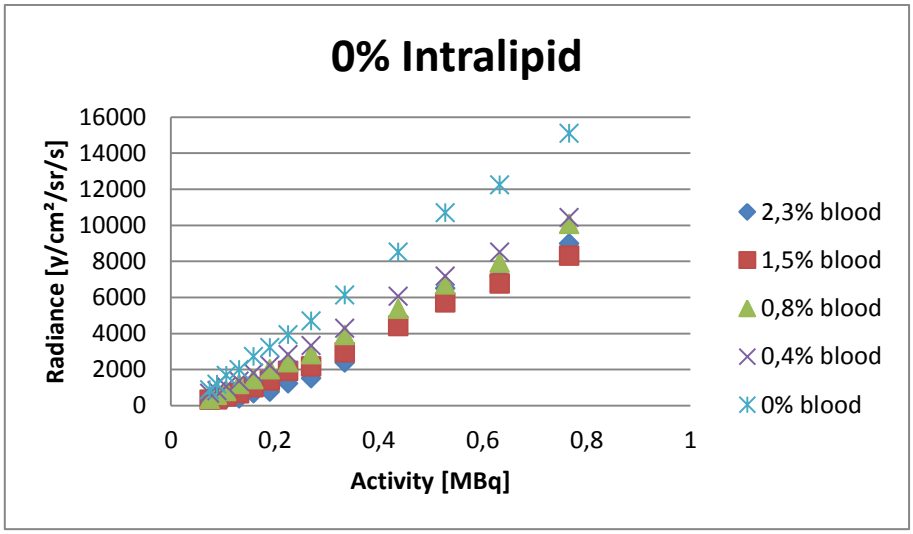

Figure 4. 7: The radiance as a function of activity for the five different blood concentrations and 0 % Intralipid.

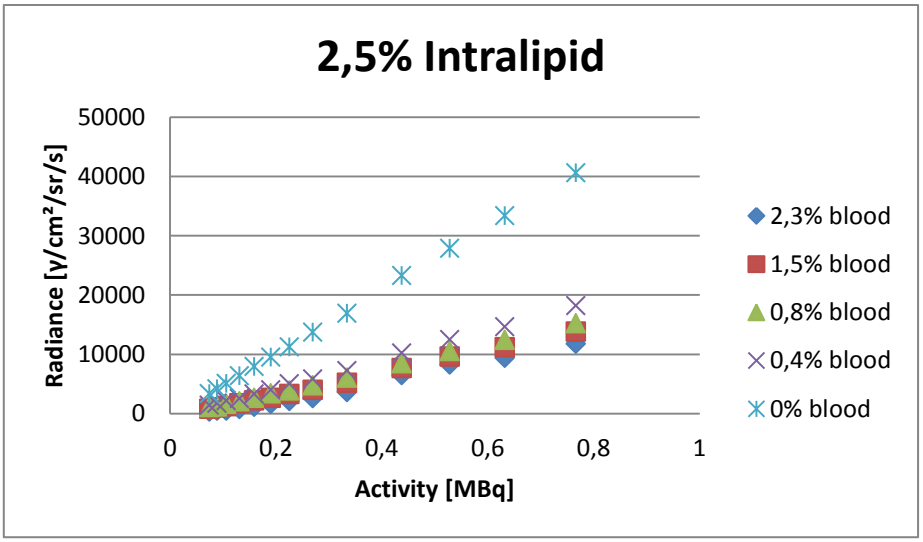

Figure 4. 8: The radiance as a function of activity for the five different blood concentrations for 2,5 % Intralipid.

The graphs in Figures 4.7 and 4.8 show that when the bovine blood is added the signal is significantly reduced. This is obviously what is expected when an absorbing agent is added to the mixture.

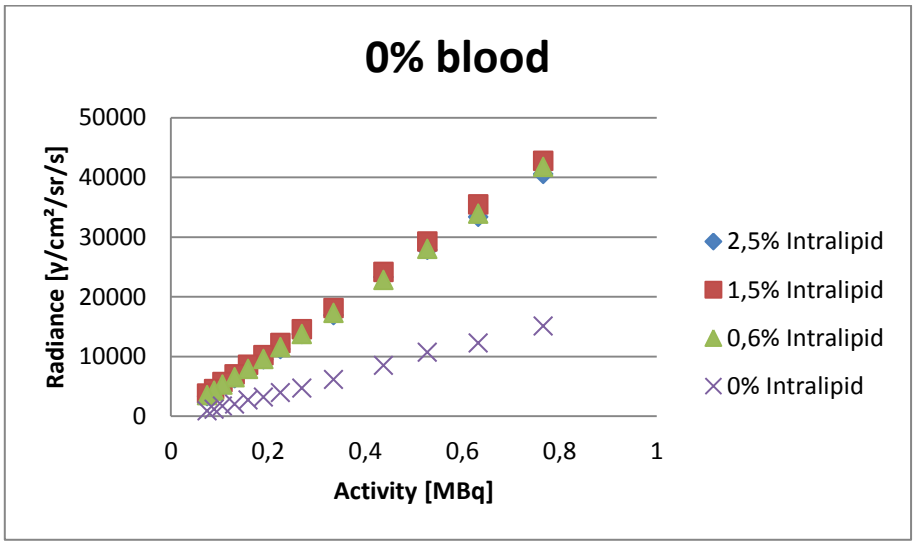

Figure 4. 9: The radiance as a function of activity for the four different concentrations of Intralipid without any blood in the mixtures.

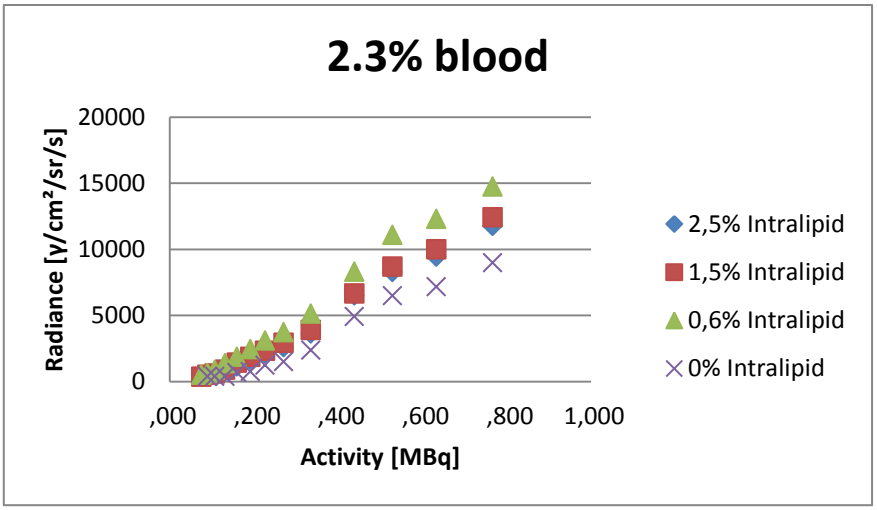

Figure 4. 10: The radiance as a function of activity for the four different percentages of Intralipid and with 2.3 % blood in the mixture.

As can be seen in Figures 4.9 and 4.10 there is an increase in radiance when a small amount of scattering material is added, however when more Intralipid is added the radiance decreases slightly with the amount of added scattering material.

4.3 Influence of absorption on quantification

The radiance per MBq was calculated and plotted against the concentration of bovine blood; this plot can be seen in Figure 4.11. The results of our measurements show that the radiance of the Cherenkov light decreases exponentially with increasing blood concentration. According to the Beer-Lambert law, see Eq. (5), this is expected for a non-scattering solution.

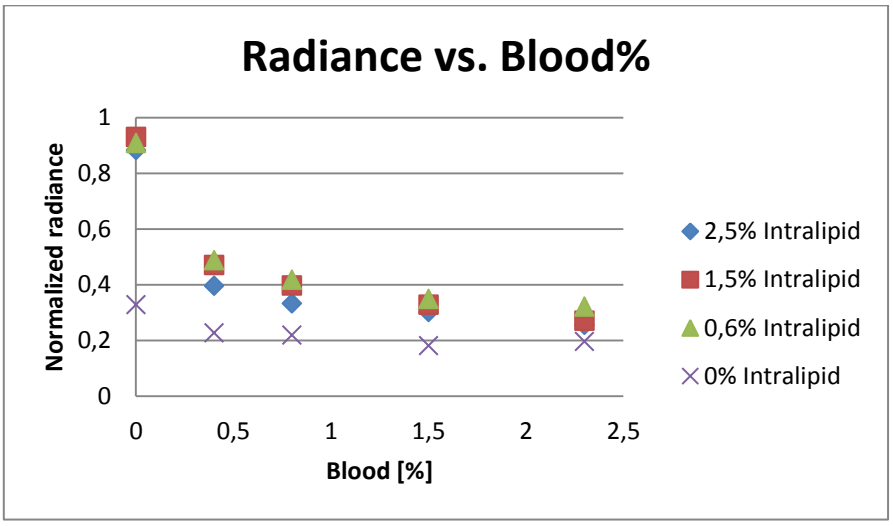

Figure 4. 11: Radiance per MBq as a function of the blood concentration for the four different percentages of Intralipid.

4.4 Influence of scattering on quantification

The radiance per MBq was plotted as a function of the percentage of Intralipid in the mixture for different levels of blood concentration, see Figure 4.12. The graph shows that a small amount of Intralipid gives rise to a higher signal, but for larger concentrations the Intralipid lowers the signal.

The scattering will increase when Intralipid is added to the solution and as a result the propagation length of the optical photons will be longer. Photons that should have been lost through the sides and the bottom of the well will with an increased scattering have a higher probability of scattering in the direction towards the camera. When the concentration of Intralipid is increased further the scattering will result in a higher attenuation, which in turn will give a decreased inclination.

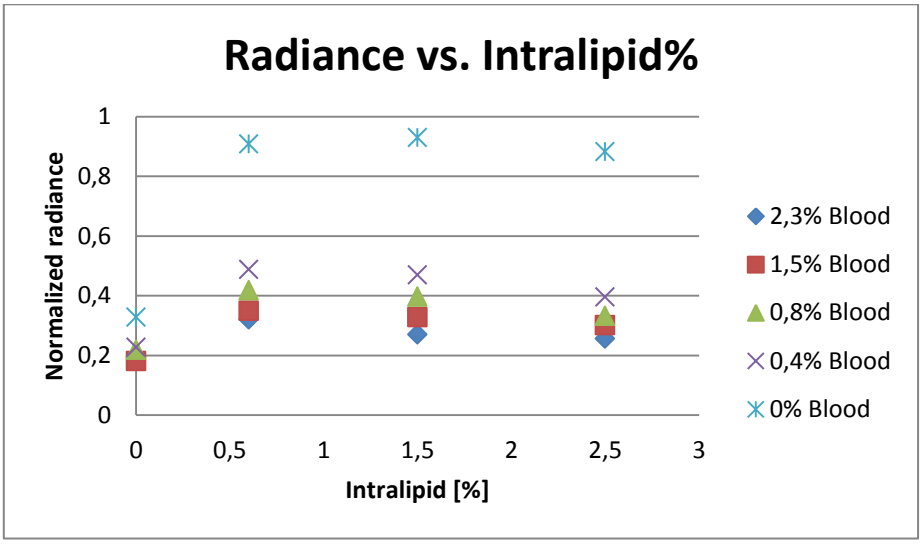

Figure 4. 12: Radiance per MBq as a function of the concentration of Intralipid for the five different blood levels.

4.5 Optical radiance as a function of the wavelength of light

To investigate the wavelength dependence of the radiance images were gathered with different filters inserted between the well plate and the CCD. This was done for a well plate containing only water and a well plate with the same mixture of water, blood and Intralipid in all the wells. As can be seen in Figure 4.13 the expected $1/\lambda^2$ dependency was achieved for the measurements with water in the wells and for the measurements with a mixture of water, bovine blood and Intralipid.

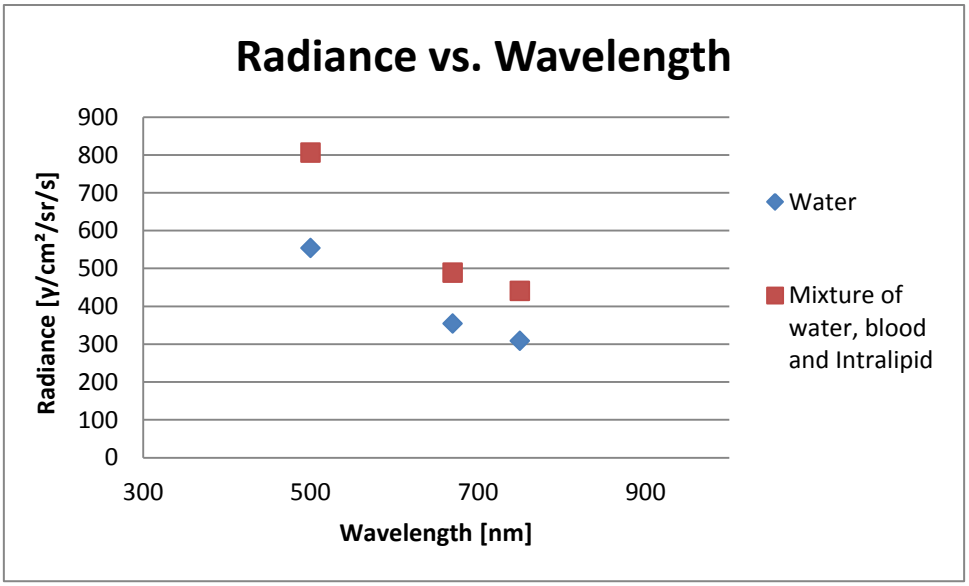

Figure 4. 13: The wavelength dependency of radiance for ^{18}F in water (blue) and in a mixture of 1200 µl water, 10 µl of bovine blood and 100 µl Intralipid (red).

4.6 Energy dependence of radiance

An optical phantom consisting of a test tube at different depths in a larger container with different amounts of absorbing and scattering material was used for these experiments; the experimental setup was presented in Figure 4.5. Two different radionuclides were used, ^{18}F and ^{89}Zr, with maximal positron energies of 634 keV and 905 keV respectively. The beta spectra for the used nuclides are presented in Figure 4.14 [31].

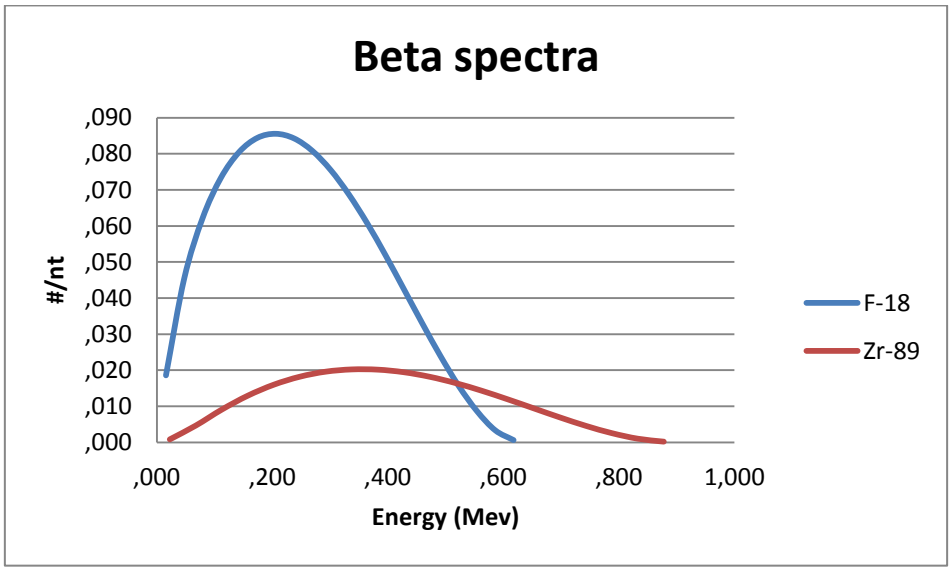

Figure 4. 14: The beta spectra for ^{18}F and ^{89}Zr, data from RADAR [31].

In Figures 4.15 and 4.17 Cherenkov emission images of the test tube containing the different nuclides at different depths in the phantom are shown and in Figures 4.16 and 4.18 a line profile of the test tubes are presented. Some useful data for a comparison of the nuclides are presented in Table 4.2.

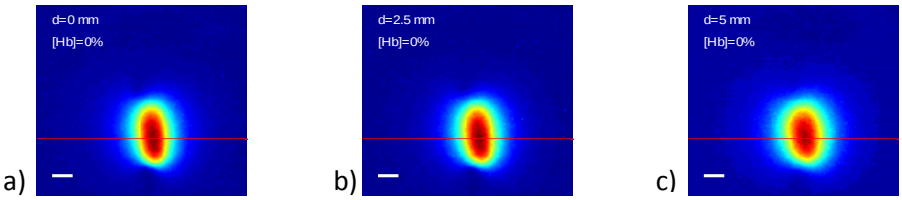

Figure 4. 15: Cherenkov emission images of a test tube containing ^{18}F, at a) 0 mm depth, b) 2.5 mm depth and c) 5mm depth in a liquid phantom. The red dotted line shows the placement of the line profile of the test tube; the profile is seen in Figure 4.16.

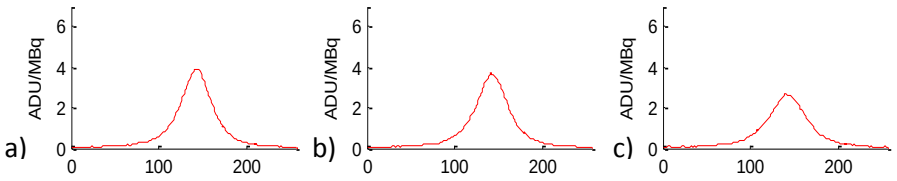

Figure 4. 16: The line profile of the test tube from Figure 4.15 containing ^{18}F.

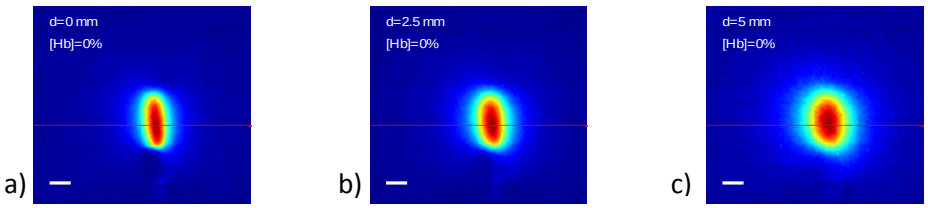

Figure 4. 17: Cherenkov emission images of a test tube containing ^{89}Zr, at a) 0 mm depth, b) 2.5 mm depth and c) 5mm depth in a liquid phantom. The red dotted line shows the placement of the line profile of the test tube; the profile is seen in Figure 4.18.

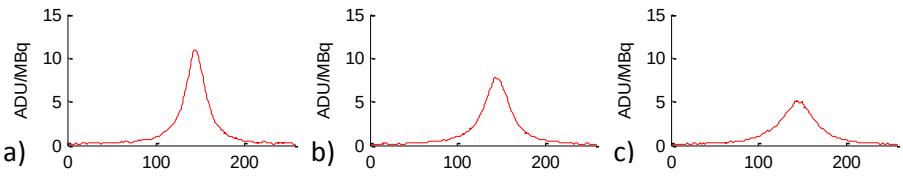

Figure 4. 18: The line profile of the test tube from Figure 4.17 containing ^{89}Zr.

By using the Cherenkov photon yields calculated by Ross et al. [10] one can obtain the maximal number of photons created by a positron with certain energies. By summarizing the photon yields for all different spectral ranges one will get the total photon yield for the nuclides. The calculation gives us that a positron with the initial energy 634 keV will produce 18,72 photons before dropping below the threshold level and a positron with an initial energy of 905 keV will produce 51,48 photons. Since we measure radiance in number of photons per square centimetre per steradian per second, a higher radiance will be detected for the nuclide with the higher energy, simply because it produces a larger number of photons.

Table 4. 2: Data for the different nuclides.

Nuclide comparison		
Nuclide	**^{18}F**	**^{89}Zr**
Mean energy [keV]	250	397
Max. energy [keV]	634	905
Max. ADU	3,9	10,84
Cherenkov photon yield	18,72	51,48

5. Cherenkov emission in vivo

5.1 Study design

In the in vivo experiments nude mice with HER2-expressing SKOV-3 xenografts were studied. The nude mice were injected with ^{89}Zr-Df-Trastuzumab and PET-images of the mice were taken 2 days post injection. Tree days post injection Cherenkov emission images of the mice were retrieved, before the mice were dissected and images of the organs were acquired. The activities in the organs were then measured with a gamma counter, and a comparison was made between the PET and Cherenkov images. There also was a comparison made between the activity measurements and the response in the Cherenkov emission images.

The exposure time for the Cherenkov emission images was 600 s.

To calibrate the system a test tube containing 0.84 MBq of ^{89}Zr was used, the Cherenkov emission image of this test tube is shown in Figure 5.1. The hot spot in the lower left corner is probably due to activity trapped in the silicone used to seal the tube and the reason for the lack of signal between the hot spot and the rest of the test tube is a piece of black tape on the test tube.

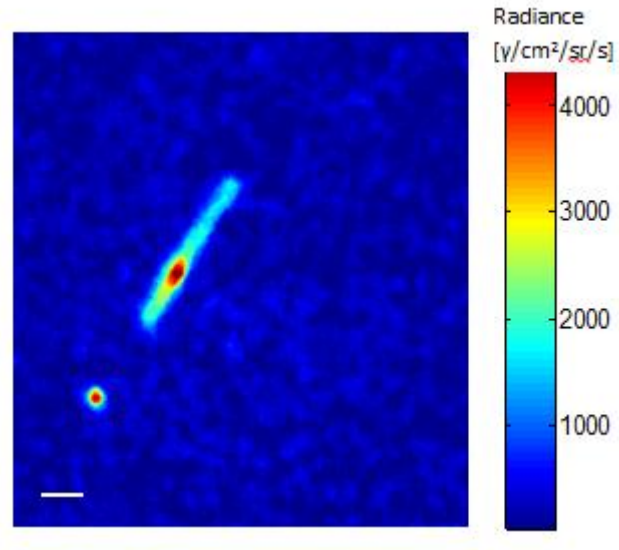

Figure 5. 1: A Cherenkov emission image of the test tube used for calibration of the system.

5.2 Whole body small animal Cherenkov emission imaging

The mice were placed in a light tight enclosure for Cherenkov emission imaging; images of the mice were then gathered for 600 s. with a CCD. A photograph and the Cherenkov emission image of the mice are shown in Figure 5.2 a) and Figure 5.2 b). As can be seen in the Cherenkov emission image most of the activity administered to mouse no 6 has ended up in the tail of the mouse, which is an indication of extravasation.

a) 

b) 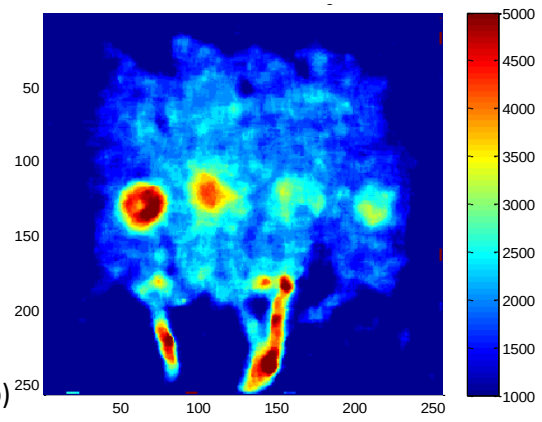

Figure 5. 2: a) (left): Mouse 4, 5, 6 and 1 before placed in the dark box for imaging. b) (right): The Cherenkov emission image of the mice, the colour bar indicates the radiance [γ/cm^2/sr/s].

In the Cherenkov emission images one region of interest was drawn over the tumour area and another at the skin surface on each mouse. The mean radiance of all these regions of interest and the tumour to skin ratio of the radiance is presented in Table 5.1.

Table 5. 1: Mean radiance for tumour and skin regions of interest, and the ratio between tumour and skin radiances.

Whole body			
Mouse	ROI	Mean radiance [γ/cm²/sr/s]	$\frac{Tumour}{Skin}$
1	Tumour	2239,5	1,6102
	Skin	1390,8	
2	Tumour	3192,5	2,2900
	Skin	1394,1	
3	Tumour	2899,4	1,7446
	Skin	1661,9	
4	Tumour	3271,6	3,3662
	Skin	971,9	
5	Tumour	2463,5	1,8399
	Skin	1338,9	
6	Tumour	1972,3	1,5942
	Skin	1237,2	

PET-images of the mice were also acquired, see Figure 5.3, and a comparison was made between the Cherenkov emission imaging and the PET-imaging. In addition the organs from two of the mice were taken out, Cherenkov emission images were taken and the activity was measured with a gamma counter, these measurements are further discussed in section 5.3.

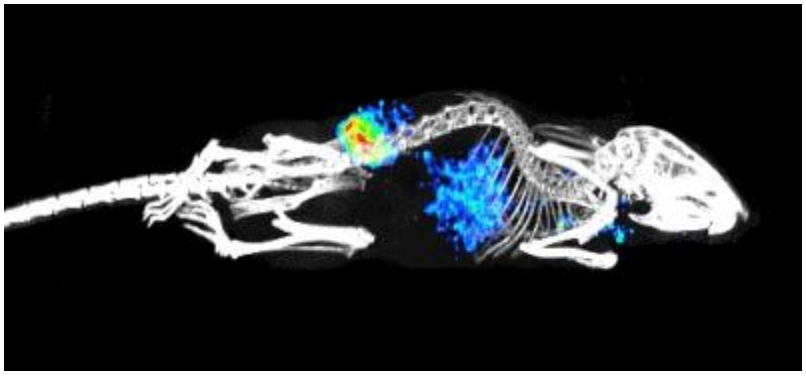

Figure 5. 3: PET-image of mouse number 1, with an uptake of ^{89}Zr seen in the tumour and in the liver.

5.3 Ex vivo organ Cherenkov emission imaging

In addition to the in vivo measurements, an ex vivo study of the animals was made. For this study two of the mice were dissected and Cherenkov emission images of the following organs were removed; heart, lungs, liver, spleen, kidneys, tumour, skin and muscle. This study was made partly because of the limited range of the Cherenkov light, in an ex vivo study it is possible to detect an uptake in organs located deeper inside the body. A photo of the extracted organs is seen in Figure 5.4 and a Cherenkov emission image of the same organs can be seen in Figure 5.5.

Figure 5. 4: The organs taken from one of the dissected mice. Top row from the left; heart, lungs, liver and spleen. Bottom row from the left; kidneys, tumour, skin and muscle.

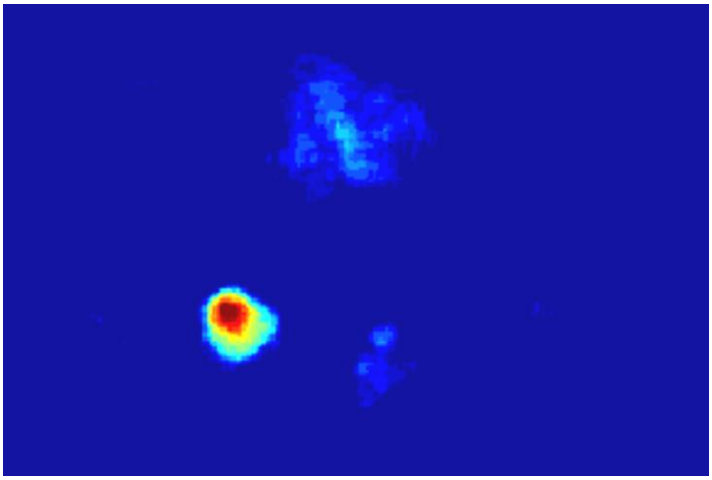

Figure 5. 5: Cherenkov emission image of the organs seen in Figure 5.4. An uptake of zirconium is seen in the liver, the tumour and in the skin.

In the ex vivo Cherenkov emission image an uptake of ^{89}Zr is seen in the liver, this is not seen in the in vivo images due to the absorption when the emitted light travels through the body.

Regions of interest were drawn over the organs in the Cherenkov emission images, the radiance in these regions was measured and the liver to tumour ratio and the tumour to skin ratio was calculated. In Table 5.2 the mean radiance of the interesting organs and the calculated ratios can be seen.

Table 5. 2: The mean radiance of the organs, the calculated liver to tumour ratio and the calculated tumour to skin ratio.

Organs				
Mouse	Organ	Mean radiance [γ/cm²/sr/s]	$\frac{Tumour}{Liver}$	$\frac{Tumour}{Skin}$
4	Tumour	2436	4,64	
	Liver	525		
1	Tumour	2144	2,2218	
	Liver	965		
2	Tumour	2759		1,8689
	Skin	1476		
3	Tumour	822		0,9712
	Skin	846		

To be able to make an attempt to quantify the Cherenkov emission images the activities of the organs were measured with a gamma counter; the measured activities are displayed in Table 5.3 below.

Table 5. 3: The measured activities in the organs from mouse number one and mouse number four.

Mouse 1		**Mouse 4**	
Organ	**Activity [kBq]**	**Organ**	**Activity [kBq]**
Heart	0,72	Heart	0,45
Lungs	3,9	Lungs	2,14
Liver	25,74	Liver	14,50
Spleen	1,11	Spleen	0,86
Kidneys	5,41	Kidneys	3,68
Tumour	9,77	Tumour	15,61
Skin	1,07	Skin	0,68
Muscle	0,59	Muscle	0,1

The measured activities were compared to the mean radiances from the Cherenkov emission images. Because of the difference in size between the tumour and the liver it is not a fair comparison to just look at the radiance and activity of the organs. Since the liver is almost six times as heavy as the tumour a direct comparison would be misleading, hence I choose to look at the radiances and activities per unit weight. In Table 5.4 one can see the measured radiance and activity, as well as the calculated radiance and activity per unit weight.

Table 5. 4: Results from the ex vivo experiments for mouse no. 1; the measured radiance and activity, and the calculated radiance and activity per unit weight.

Organ	Radiance [γ/cm²/sr/s]	Radiance/weight [γ/cm²/sr/s/g]	Activity [kBq]	Activity/weight [kBq/g]
Liver	965	569	26	15
Tumour	2144	7393	10	34

Since the liver also contains rather much blood the radiance seen is probably originating from the surface, due to the restricted range of the Cherenkov radiation in blood rich tissues. The high blood content could also explain the lower radiance per unit weight, since the blue wavelengths of the emitted Cherenkov light is heavily absorbed by it.

6. Discussion

The results shown in this thesis state that the relation between radiance and activity is linear with different inclination for different tissue types. These results confirm what has been shown by other groups and what is expected according to theory. A higher activity produces more detectable Cherenkov photons which gives a higher detected radiance, this renders Cherenkov emission imaging to potentially become an important imaging modality for longitudinal studies where the activity in an animal is monitored over a long time.

From these results one can see that the amount of added bovine blood affects the radiance more than the amount of Intralipid, indicating that the radiance is more affected by the amount of absorbing material than by the amount of scattering material in the studied object. One could from this draw the conclusion that the absorption of the light has a larger impact on the images than scattering. This fact has implications for organ imaging, which means that the Cherenkov radiance would need to be normalized against the blood content in each organ before making the relative comparison of the accumulation of a specific radionuclide in different organs. However, instrumentation for assessment of blood concentration is readily available through fiber optic broadband optical spectroscopy which means this is not a problem [20].

The theoretical $1/\lambda^2$ dependence is also verified by the shown results. Even if these results are promising, they are not statistically significant due to the fact that only one series of measurements was made in this study and we did not have the possibility to study all wavelengths of the emitted Cherenkov light.

The results from the comparison between different nuclides show that a nuclide with a higher energy gives more detectable light, which is rather obvious if you look at the table showing the number of emitted Cherenkov photons produced by beta particles of different energies [10]. Unfortunately there was no possibility to make an extensive investigation on the nuclide dependence of the radiance, but the results obtained are in good agreement with the theoretical expectations. It would have been interesting to make more experiments to obtain a larger set of data to draw conclusions from.

In this study there were no quantitative measurements made to determine the difference in spatial resolution for the two nuclides, instead a brief qualitative comparison of the images was made. The images obtained from the energy dependence measurements indicate that the spatial resolution is somewhat better for the nuclide with higher energy at small depths, since the image of the test tube looks wider for the nuclide with lower energy. For deeper positioning of the test tube there is no larger difference between the nuclides, possibly the resolution looks better for the nuclide with the lower energy.

The measurements made to investigate the relation between radiance and activity show that for all different concentrations of Intralipid and bovine blood the radiance is linearly dependent of the activity. This means that if the absorbing and scattering properties of the studied medium are fairly constant one can accomplish longitudinal studies with very good results. Reasonably the same kinetics curve for the tumour should be obtained with CLI as well as PET, SPECT or gamma counters.

7. Conclusions

Cherenkov emission imaging can be used for radionuclide localization in pre-clinical animal studies, this means that a possible application for the imaging method is to study selective uptake in (superficial) tumours over time. Another possible application for Cherenkov emission imaging could be to compare the efficiency of different monoclonal antibodies or other types of tracers in small animals.

To be able to really make quantitative measurements you need to know, or at least be able to estimate, the amount of blood in the observed organs and make corrections for this. Fortunately, there are a number of optical methods to measure blood concentrations that can help us get around this problem.

As with all new methods and approaches, the CLI method needs to be investigated further before being implemented in preclinical or clinical use. At the moment the method seems to be able to provide a low-cost high-throughput alternative to preclinical PET, at least for superficial tumours in mice and for ex vivo measurements.

8. References

1. Bomanji, J.B., *Radionuclide therapy.* Clin Med, 2006. **6**(3): p. 249-53.
2. Brumley, C.L. and J.A. Kuhn, *Radiolabeled monoclonal antibodies.* AORN J, 1995. **62**(3): p. 343-50, 353-5; quiz 356-8, 361-2.
3. Chatal, J.F. and C.A. Hoefnagel, *Radionuclide therapy.* Lancet, 1999. **354**(9182): p. 931-5.
4. Park, J.C., et al., *Luminescence imaging using radionuclides: a potential application in molecular imaging.* Nucl Med Biol, 2011. **38**(3): p. 321-9.
5. Robertson, R., et al., *Optical imaging of Cerenkov light generation from positron-emitting radiotracers.* Phys Med Biol, 2009. **54**(16): p. N355-65.
6. Axelsson, J., et al., *Cerenkov emission induced by external beam radiation stimulates molecular fluorescence.* Med Phys, 2011. **38**(7): p. 4127-32.
7. Ruggiero, A., et al., *Cerenkov luminescence imaging of medical isotopes.* J Nucl Med, 2010. **51**(7): p. 1123-30.
8. Beattie, B.J., et al., *Quantitative modeling of Cerenkov light production efficiency from medical radionuclides.* PLoS One, 2012. **7**(2): p. e31402.
9. Xu, Y., H. Liu, and Z. Cheng, *Harnessing the power of radionuclides for optical imaging: Cerenkov luminescence imaging.* J Nucl Med, 2011. **52**(12): p. 2009-18.
10. Ross, H.H., *Measurement of β-Emitting Nuclides Using Cerenkov Radiation.* Analytical Chemistry, 1969. **41**(10): p. 6.
11. Dothager, R.S., et al., *Cerenkov radiation energy transfer (CRET) imaging: a novel method for optical imaging of PET isotopes in biological systems.* PLoS One, 2010. **5**(10): p. e13300.
12. Spinelli, A.E., et al., *Cerenkov radiation allows in vivo optical imaging of positron emitting radiotracers.* Phys Med Biol, 2010. **55**(2): p. 483-95.
13. Mitchell, G.S., et al., *In vivo Cerenkov luminescence imaging: a new tool for molecular imaging.* Philosophical Transactions of the Royal Society A, 2011(369): p. 4605-4619.
14. Holland, J.P., et al., *Intraoperative imaging of positron emission tomographic radiotracers using Cerenkov luminescence emissions.* Mol Imaging, 2011. **10**(3): p. 177-86, 1-3.
15. Boschi, F., et al., *In vivo (1)(8)F-FDG tumour uptake measurements in small animals using Cerenkov radiation.* Eur J Nucl Med Mol Imaging, 2011. **38**(1): p. 120-7.
16. Robertson, R., et al., *Multimodal imaging with (18)F-FDG PET and Cerenkov luminescence imaging after MLN4924 treatment in a human lymphoma xenograft model.* J Nucl Med, 2011. **52**(11): p. 1764-9.
17. Spinelli, A.E. and F. Boschi, *Optimizing in vivo small animal Cerenkov luminescence imaging.* J Biomed Opt, 2012. **17**(4): p. 040506.
18. Sassaroli, A. and S. Fantini, *Comment on the modified Beer-Lambert law for scattering media.* Phys Med Biol, 2004. **49**(14): p. N255-7.
19. Matcher, S.J. and C.E. Cooper, *Absolute quantification of deoxyhaemoglobin concentration in tissue near infrared spectroscopy.* Phys Med Biol, 1994. **39**(8): p. 1295-312.
20. Bevilacqua, F., et al., *Broadband absorption spectroscopy in turbid media by combined frequency-domain and steady-state methods.* Appl Opt, 2000. **39**(34): p. 6498-507.
21. Cerussi, A., et al., *In vivo absorption, scattering, and physiologic properties of 58 malignant breast tumors determined by broadband diffuse optical spectroscopy.* J Biomed Opt, 2006. **11**(4): p. 044005.

22. Fedorow, H., et al., *Neuromelanin in human dopamine neurons: comparison with peripheral melanins and relevance to Parkinson's disease.* Prog Neurobiol, 2005. **75**(2): p. 109-24.
23. Bowen, W.J., *The absorption spectra and extinction coefficients of myoglobin.* J Biol Chem, 1949. **179**(1): p. 235-45.
24. Balaban, R.S., V.K. Mootha, and A. Arai, *Spectroscopic determination of cytochrome c oxidase content in tissues containing myoglobin or hemoglobin.* Anal Biochem, 1996. **237**(2): p. 274-8.
25. Mourant, J.R., et al., *Predictions and measurements of scattering and absorption over broad wavelength ranges in tissue phantoms.* Appl Opt, 1997. **36**(4): p. 949-57.
26. Bigio, I.J. and J.R. Mourant, *Ultraviolet and visible spectroscopies for tissue diagnostics: fluorescence spectroscopy and elastic-scattering spectroscopy.* Phys Med Biol, 1997. **42**(5): p. 803-14.
27. Wang, X., et al., *Approximation of Mie scattering parameters in near-infrared tomography of normal breast tissue in vivo.* J Biomed Opt, 2005. **10**(5): p. 051704.
28. Bohren, C.F. and D.R. Huffman, *Absorption and Scattering of Light by Small Particles*2008: John Wiley & Sons Inc.
29. van Staveren, H.J., et al., *Light scattering in Intralipid-10% in the wavelength range of 400-1100 nm.* Appl Opt, 1991. **30**(31): p. 4507-14.
30. FDA, *Intralipid 20% Label information*, 2007: http://www.accessdata.fda.gov/drugsatfda_docs/label/2007/017643s072,018449s039lbl.pdf.
31. Stabin, M.G. *RADAR - the RAdiation Dose Assessment Resource*. Available from: http://www.doseinfo-radar.com/RADARDecay.html.